Multiple critical points and liquid–liquid equilibria from the van der Waals like equations of state

2008 J. Phys.: Condens. Matter 20 244119

(http://iopscience.iop.org/0953-8984/20/24/244119)

IOP PUBLISHING JOURNAL OF PHYSICS: CONDENSED MATTER

J. Phys.: Condens. Matter **20** (2008) 244119 (8pp) doi:10.1088/0953-8984/20/24/244119

Multiple critical points and liquid–liquid equilibria from the van der Waals like equations of state

Sergey Artemenko, Taras Lozovsky and Victor Mazur[1]

Thermodynamics Department, Academy of Refrigeration, 65082 Odessa, Ukraine

Received 31 March 2008
Published 29 May 2008
Online at stacks.iop.org/JPhysCM/20/244119

Abstract

The principal aim of this work is a comprehensive analysis of the phase diagram of water via the van der Waals like equations of state (EoSs) which are considered as superpositions of repulsive and attractive forces. We test more extensively the modified van der Waals EoS (MVDW) proposed by Skibinski *et al* (2004 *Phys. Rev.* E **69** 061206) and refine this model by introducing instead of the classical van der Waals repulsive term a very accurate hard sphere EoS over the entire stable and metastable regions (Liu 2006 *Preprint* cond-mat/0605392). It was detected that the simplest form of MVDW EoS displays a complex phase behavior, including three critical points, and identifies four fluid phases (gas, low density liquid (LDL), high density liquid (HDL), and very high density liquid (VHDL)). Moreover the experimentally observed (Mallamace *et al* 2007 *Proc. Natl Acad. Sci. USA* **104** 18387) anomalous behavior of the density of water in the deeply supercooled region (a density minimum) is reproduced by the MWDW EoS. An improvement of the repulsive part does not change the topological picture of the phase behavior of water in the wide range of thermodynamic variables. The new parameters set for second and third critical points are recognized by thorough analysis of experimental data for the loci of thermodynamic response function extrema.

(Some figures in this article are in colour only in the electronic version)

1. Introduction

The attempts to discover *in vivo* more than two different disordered equilibrium phases and their respective critical points in one-component fluids is confronted by the lack of reliable estimations of the state parameters where new phenomena can be observed. Water is one vivid example of a molecular system where quite different structures are formed *in vitro* by computer simulation but needs experimental verification. At the moment the complete phase diagram of water is still missing and experimental proof of second and third critical points is a subject of debate.

Experimental data about liquid–liquid phase transitions published over the last decade have confirmed surprising behavior for a diversity of single-component systems such as carbon [1, 2], phosphorous [3–5], triphenyl phosphite [6, 7], silica [8], nitrogen [9], and water [10–14]. A great many explanations of multicriticality in monocomponent fluids (perturbation theory models [15, 16], semiempirical models [17–20], lattice models [21–23], two-state models [24–26], field theoretical models [27], two-order-parameter models [28–32], and parametric crossover models [33]) have been disseminated following the pioneering work by Hemmer and Stell [34]. Detailed discussions of different *pro et contra* exploratory scenarios of water behavior have been published in the thorough reviews [35–37]. It should be noted that anomalous behavior of thermodynamic variables and their derivatives is not only the prerogative of water. Liquid helium isotopes also exhibit non-conventional properties at very low temperature (maximum density, the Pomeranchuk's effect in liquid He^3, temperature decreasing under adiabatic compression, etc). The main mechanism of unusual from daily experience but thermodynamically correct behavior of different substances is a competition of entropic measures among inherent clandestine structures at given state parameters.

A fundamental contradiction associated with the impracticality to obtain a reliable prediction of thermodynamic and phase behavior of substances from first principles and the

[1] Author to whom any correspondence should be addressed.

necessity to introduce the computationally feasible simplifications is overcome in general by the parametrization of models and their consequent fitting to experimental data. Such models offer the useful tools of aggregating large data sets, allowing us to extend data beyond regions in which measurements have been made, and providing insight into physical phenomena. However, the transition from real phenomenon to its model entails the appearance of uncertainty sources caused by the statistical pattern of experimental information, inadequacy and ambiguity of used models due to estimation of parameters from experimental data, which are generated by different experimental units possessing as a rule different dimensions, different physical meaning, and different statistical distribution. It results in a conflict situation when the set of parameters restored according to one category of data does not correspond to parameters from other data sources. Therefore, the conflict appears in model parameter estimation and it is desirable to reduce an arising uncertainty by the simultaneous consideration of all available data.

A first step in the quantitative description of real phenomena is a selection of the model that can qualitatively describe a variety of thermodynamic surface anomalies of water over a wide range of temperatures and pressures. The principal aim of this work is a comprehensive analysis of the phase diagram of water via the van der Waals like equations of state (EoSs) which are considered as a superposition of repulsive and attractive forces. Here we test more extensively the modified van der Waals EoS (MVDW) proposed in [20] and refine this model by introducing instead of the classical van der Waals repulsive term a very accurate hard sphere EoS over the entire stable and metastable regions [38]. This paper is structured as follows. In section 2 we review the MVDW model proposed by Skibinsky *et al* [20] and take into account the more exact hard sphere term from Liu's paper [38]. Section 3 displays the picture of the phase behavior for different parameters of the MVDW model, and the third critical point, which had no evidence earlier for this model, is clearly established. It allows us to interpret four fluid phases as gas, low density liquid (LDL), high density liquid (HDL), and very high density liquid (VHDL). Moreover the anomalous behavior of the density of water in the deeply supercooled region (a density minimum) experimentally observed by Mallamace *et al* [39] is reproduced by MWDW EoS. It is demonstrated that improvement of the repulsive part does not change a topological picture of the phase behavior of water in the wide range of thermodynamic variables. In section 4 analysis of experimental data both for the loci of extrema of thermodynamic response functions and at an intersection of isotherms in the metastable region as a result of multiextrema density behavior allowed us to forecast the new critical parameters for a second critical point.

2. Thermodynamic model

A mean field EoS is a major tool for the description of general thermodynamic behavior in the existence domain of state variables. The various physical approximations do not change the topological structure of the thermodynamic surface which is generated by mean field theories. For this reason the simplest models of the van der Waals like EoS demonstrating the great variety of features of thermodynamic and phase behavior for mono and multicomponent fluids were chosen. The total compressibility factor is expressed as the sum of repulsive and attractive parts

$$Z = Z_{\text{rep}} + Z_{\text{attr}}. \tag{1}$$

To compare very accurate and very rough approximations for the repulsive term, the classical van der Waals expression

$$Z = \frac{1}{1-4\eta} \tag{2}$$

and the wide range hard sphere EoS for stable and metastable regions from [38]

$$Z_{\text{rep}} = 1 + \sum_{i=1}^{12} a_{i+1}\eta^i + \frac{c_0\eta}{1-\alpha\eta} + c_1\eta^{40} + c_2\eta^{42} + c_3\eta^{44} \tag{3}$$

are used.

Here $Z = PV/NkT$ is the compressibility factor, and P, the pressure, V, the total volume, T, the temperature, N, the total number of particles, k, the Boltzmann constant, η, the packing fraction, defined as $\eta = \pi\rho d^3/6$, $\rho = N/V$, the number density and d, the hard sphere diameter. The coefficients a_i ($i = 1, 2, \ldots, 12$) and c_i ($i = 0 \ldots 3$) were taken from [38] and reproduce the virial coefficients up to the 12th term. The most important parameter for the metastable region is $\alpha = 1/0.635\,584$. The inverse value gives the maximally random jammed packing and places a limit of EoS applicability that is very close to the computer simulation result $\eta_0 = 0.6418$.

The attractive term has the same form as the classical van der Waals EoS expression

$$Z_{\text{attr}} = -\frac{A\eta}{NkT} \tag{4}$$

where A is the interaction constant.

The conventional van der Waals approach where model parameters d and A are the constants cannot describe more than one first-order phase transition and one critical point. Therefore a key question is a formulation of temperature–density dependency for EoS parameters generating more than one critical point in the monocomponent matter. There are several approaches of the effective hard sphere determination from spherical interaction potential models that have a region of negative curvature in their repulsive core (the so-called core softened potentials). To avoid the sophistication of EoS and study a qualitative picture of phase behavior we adopt the approach of Skibinsky *et al* [20] for a one-dimensional system of particles interacting via pair potential

$$U(R) = \begin{cases} \infty, & R < d_{\text{h}} \\ U_R/U_A, & d_{\text{h}} < R < d_{\text{s}} \\ 0, & R > d_{\text{s}} \end{cases} \tag{5}$$

where d_{h} is a diameter associated with a hard core, d_{s} is a diameter associated with the impossibility of a particle

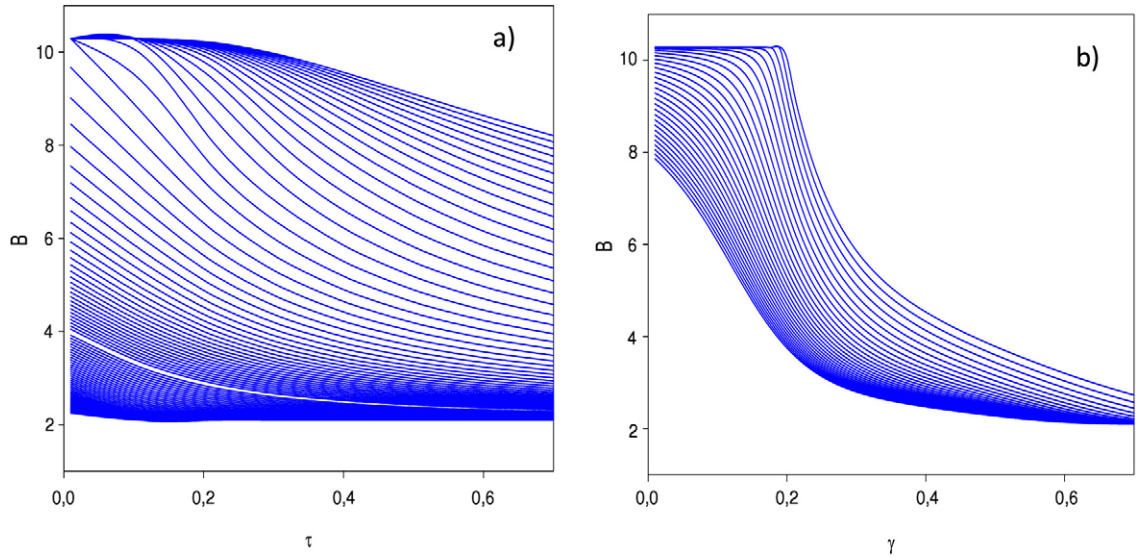

Figure 1. The temperature (a) and density (b) dependence of the excluded volume for the model parameter set: $d_h = 2.27$, $U_R = 2$, $d_s = 10.29$. (a) B-curves correspond to isochores for $\gamma = B_h\rho$ from 0.01 (top) to 0.9 (bottom) with step 0.01, (b) B-curves correspond to isotherms for $\tau = kT/U_R$ from 0.01 (top) to 0.9 (bottom) with step 0.025.

to penetrate into the soft core at low densities and low temperatures.

The algorithm excluded volume $B_i(\rho, T) = \frac{2}{3}\pi d_i^3$, $i =$ h, s calculation is given in [38]. The behavior of the excluded volume in the entire range of densities and temperatures is illustrated in figure 1.

3. Phase diagrams

The opportunity to locate fluid–fluid phase transitions depends on the concurrence between the repulsive and the attractive parts of the EoS. In this paper we adduce the new features of the mean field model EoS (1) for the simplest interaction potential (5) to explain the anomalous behavior of the thermodynamic surface of water. The binodal location at given temperature, T, and pressure, P, is a solution of the set of equations:

$$\begin{aligned} \mu(\rho', T) - \mu(\rho'', T) = 0 \\ p(\rho', T) - p(\rho'', T) = 0 \end{aligned} \tag{6}$$

where ρ' and ρ'' are the densities of the coexisting phases, the pressure, p, is calculated from the EoS described, the expression for the chemical potential, μ, can be derived from an EoS using standard thermodynamic relations. Spinodals are determined via the following thermodynamic condition:

$$\left(\frac{\partial p}{\partial V}\right)_T = 0. \tag{7}$$

Figures 2–7 show the phase behavior for the van der Waals EoS where diameter depends on state variables. The appearance of a third critical point with repulsive term (2) was detected which surprisingly broadens the possibilities of a very simple EoS model. Water is known to have both low density and high density amorphous phases, which can be transformed from one to the other by changing pressure at low temperatures. It therefore allows us to consider the liquid state as a mixture of the two corresponding fluid phases, LDL and HDL. The HDL has the local tetrahedrally coordinated hydrogen bonded (HB) structure, whereas the LDL holds locally the 'ice-like' HB network. The availability of a third critical point at high densities allows us to surmise that a near fivefold increase of the gas–liquid critical density for water identifies the very dense liquid phase (VHDL) discovered recently. Figure 5 illustrates a possible scenario of the isotherm behavior in the P–T phase diagram for the core softened potential with the third critical point in the metastable region. This result confirms a suggestion that HDL is not stable but rather is a highly metastable structure, relaxing to VHDL as glasses generated with hyperquenched methods relax on slow heating to glasses generated with conventional cooling rates [40].

An improvement of a classical repulsive expression (2) for a one-dimensional system of hard spheres by the very accurate presentation of the Liu EoS [38] (figure 7) does not change the topological picture of the phase diagram in comparison with the classical van der Waals expression. It seems that an improvement of the repulsive term makes more soundness of isotherm behavior near the second critical point. To analyze a qualitative behavior of thermodynamic surface anomalies as a whole the simpler model is preferable due to a topological equivalence of the models under consideration.

4. Density anomalies and position of the second critical point

There are different discordant scenarios of the second critical point disclosure in the pressure–temperature diagram but true parameters of singularity remain very vague. Figure 8 illustrates the scattering of values of the second critical point position among different authors [33, 35, 41–47]. A most reliable method of critical point estimation is based on the

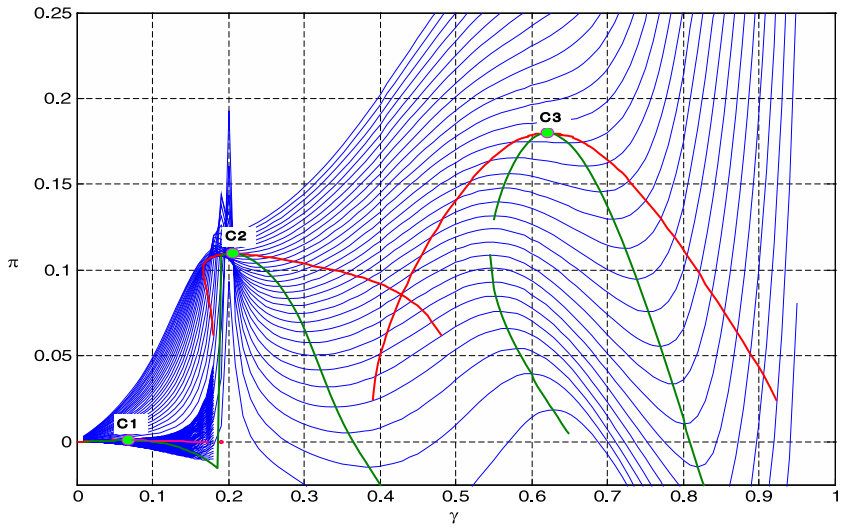

Figure 2. Evolution of isotherms in the P–ρ phase diagram for the core softened potential with three critical points: C1—gas + liquid, C2—LDL + HDL, and C3—HDL + VHDL. Red curves (online) are coexistence curves; green curves (online) are spinodals. Critical point location: $\pi_{C1} = 0.832 \times 10^{-3}$, $\tau_{C1} = 0.0327$, $\gamma_{C1} = 0.0678$; $\pi_{C2} = 0.1096$, $\tau_{C2} = 0.2297$, $\gamma_{C2} = 0.2060$; $\pi_{C3} = 0.1799$, $\tau_{C3} = 0.1746$, $\gamma_{C3} = 0.6210$. Model parameter set: $A = 2.272$, $U_R/U_A = 2$, $B_s = 10.2898$, $B_s/B_h = 4.913$.

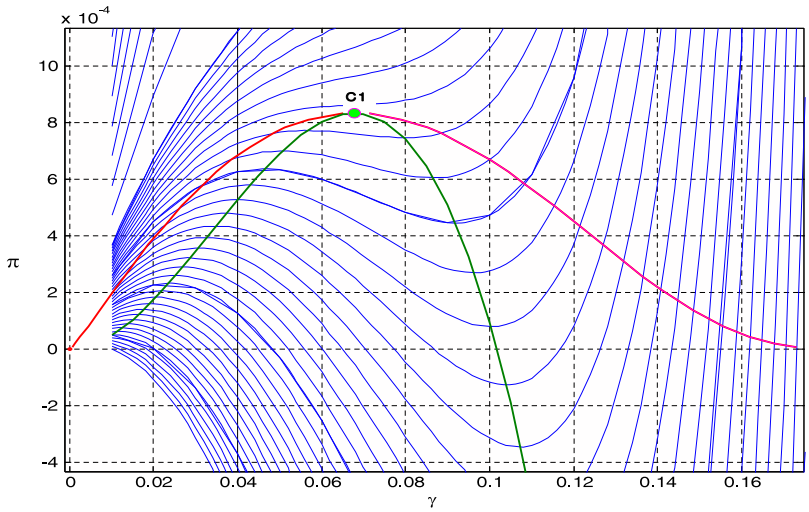

Figure 3. Evolution of isotherms in the P–ρ phase diagram near gas + liquid critical point. C1—gas + liquid. Red lines (online) are coexistence curves; green lines (online) are spinodals. Critical point location: $\pi_{C1} = 0.832 \times 10^{-3}$, $\tau_{C1} = 0.0327$, $\gamma_{C1} = 0.0678$; $\pi_{C2} = 0.1096$, $\tau_{C2} = 0.2297$, $\gamma_{C2} = 0.2060$; $\pi_{C3} = 0.1799$, $\tau_{C3} = 0.1746$, $\gamma_{C3} = 0.6210$. Model parameter set: $A = 2.272$, $U_R/U_A = 2$, $B_s = 10.2898$, $B_s/B_h = 4.913$.

density fluctuation data analysis as a tool for quantitative and direct identification of the inhomogenity from the viewpoint of mesoscopic and macroscopic states. The density fluctuations form a ridge which deviates slightly from the critical isochore not so far from the critical point [49]. The ridge corresponds to extrema for heat capacity, isothermal compressibility, partial molar volumes, sound velocity, and thermal conductivity (the so-called Widom lines). For example, the intersection of maximum isobaric heat capacity $C_P^{\max}$ and maximum isothermal compressibility $k_T^{\max}$ lines in the pressure–temperature phase diagram localizes the critical point position quite accurately. The main problem of the computer simulations of the thermodynamic behavior of water is the very large discrepancies between experimental data and calculations via the popular water model TIP5P [50]. To illustrate quantitatively the existing discrepancies we have compared in table 1 the simulation data from [51] and 'experimental' data calculated from the very accurate EoS proposed by Pruß and Wagner (The IAPWS Formulation 1995 for the Thermodynamic Properties of Ordinary Water Substance for General and Scientific Use) [48]. The uncertainty in density of the IAPWS-95 EoS is 0.0001% at 1 atm in the liquid phase, and 0.001% at other liquid states at pressures up to 10 MPa and temperatures to 423 K. The uncertainties rise at higher temperatures and/or pressures, but are generally less than 0.1% in density except at extreme conditions. The uncertainty in isobaric heat capacity is 0.1% in the liquid phase.

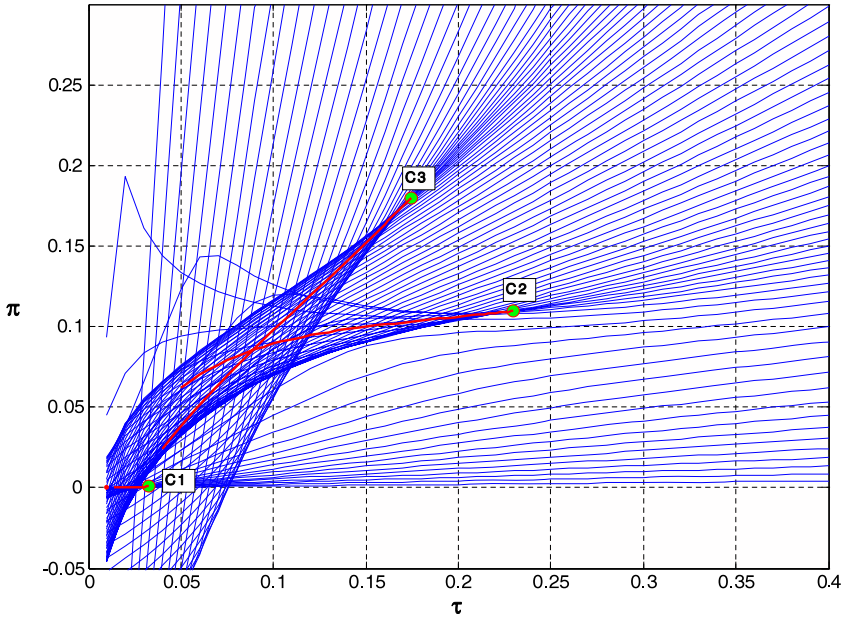

Figure 4. Evolution of isochores in the P–T phase diagram for the core softened potential with three critical points: C1—gas + liquid, C2—LDL + HDL, and C3—HDL + VHDL. Red lines (online) are coexistence curves. Critical point location: $\pi_{C1} = 0.832 \times 10^{-3}$, $\tau_{C1} = 0.0327$, $\gamma_{C1} = 0.0678$; $\pi_{C2} = 0.1096$, $\tau_{C2} = 0.2297$, $\gamma_{C2} = 0.2060$; $\pi_{C3} = 0.1799$, $\tau_{C3} = 0.1746$, $\gamma_{C3} = 0.6210$. Model parameter set: $A = 2.272$, $U_R/U_A = 2$, $B_s = 10.2898$, $B_s/B_h = 4.913$.

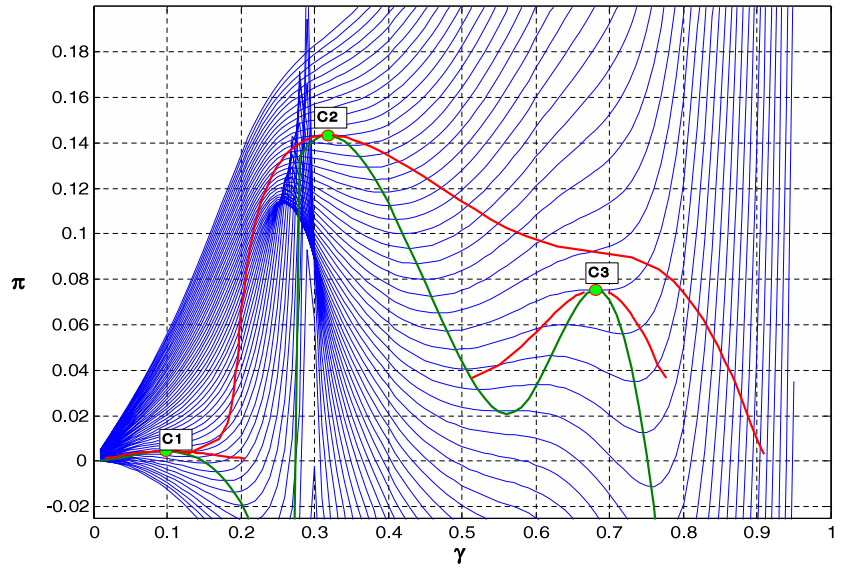

Figure 5. Evolution of isotherms in the P–ρ phase diagram for the core softened potential with the third critical point in the metastable region: C1—gas + liquid, C2—LDL + HDL, and C3—HDL + VHDL critical points. Red lines (online) are coexistence curves; green lines (online) are spinodals. Critical point location: $\pi_{C1} = 4.326 \times 10^{-3}$, $\tau_{C1} = 0.1168$, $\gamma_{C1} = 0.0988$; $\pi_{C2} = 0.1434$, $\tau_{C2} = 0.3852$, $\gamma_{C2} = 0.3177$; $\pi_{C3} = 0.0755$, $\tau_{C3} = 0.2451$, $\gamma_{C3} = 0.6815$. Model parameter set: $A = 6.962$, $U_R/U_A = 3$, $B_s = 7.0686$, $B_s/B_h = 3.375$.

The uncertainty of computer simulation data corresponding to the relative deviations (RD) mentioned from table 1 in terms of temperature scale gives an estimation of the uncertainty ∼40–50 K. In figure 8 we also show that the dependence of the maximum of isobaric heat capacity from molecular dynamics (MD) simulations [52] has a similar shift compared to calculations of the Widom line from the IAPWS-95 EoS [48] at the same pressures and temperatures. To apply the computer simulation results we need to rescale their values.

The van der Waals like models cannot predict correctly the anomalous behavior of mechanical and thermal response functions due to fundamental restrictions of the mean field approximation. The divergence of the response functions in the vicinity of the second critical point in water is essentially weaker than near the liquid–vapor critical point where the response functions diverge more strongly [44]. This fact complicates the search for the second critical point both for theoretical and experimental methods. The final conclusion

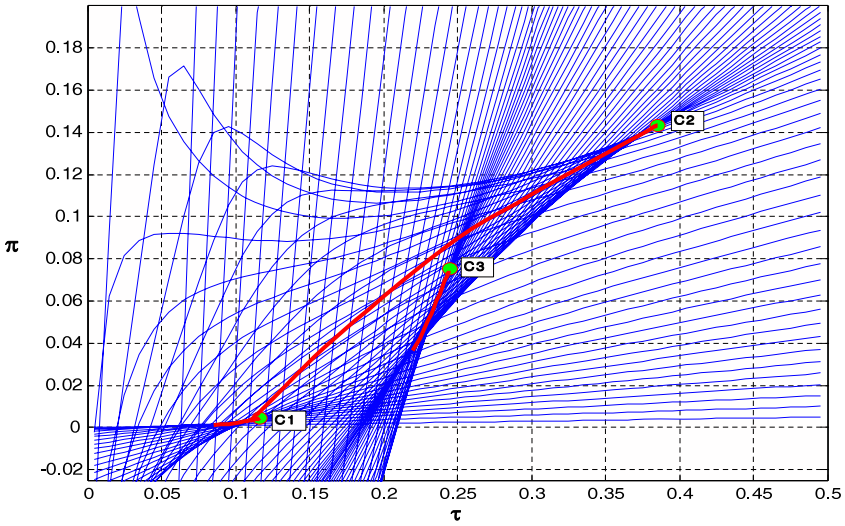

Figure 6. Evolution of isochores in the P–T phase diagram for the core softened potential with the third critical point in metastable region: C1—gas + liquid, C2—LDL + HDL, and C3—HDL + VHDL critical points. Red lines (online) are coexistence curves. Blue curves (online) are isochores. Critical point location: $\pi_{C1} = 4.326 \times 10^{-3}$, $\tau_{C1} = 0.1168$, $\gamma_{C1} = 0.0988$; $\pi_{C2} = 0.1434$, $\tau_{C2} = 0.3852$, $\gamma_{C2} = 0.3177$; $\pi_{C3} = 0.0755$, $\tau_{C3} = 0.2451$, $\gamma_{C3} = 0.6815$. Model parameter set: $A = 6.962$, $U_R/U_A = 3$, $B_s = 7.0686$, $B_s/B_h = 3.375$.

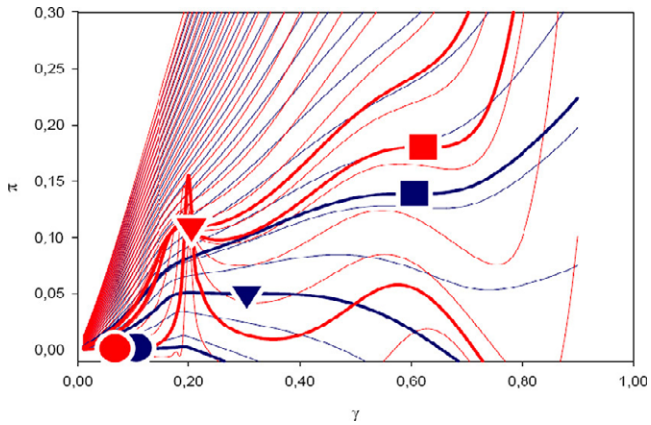

Figure 7. Evolution of isotherms in the P–ρ phase diagram from the core softened potential with three critical points. The filled circles are the C1—gas + liquid critical point, the triangles correspond to the C2—LDL + HDL second critical point, and squares are the C3—HDL + VHDL critical point. Blue curves (online) are isotherms according to the van der Waals EoS with Liu's repulsive term. Critical point location: $\pi_{C1} = 1.5824 \times 10^{-3}$, $\tau_{C1} = 0.0416$, $\gamma_{C1} = 0.1059$; $\pi_{C2} = 0.0501$, $\tau_{C2} = 0.1597$, $\gamma_{C2} = 0.3049$; $\pi_{C3} = 0.1389$, $\tau_{C3} = 0.2708$, $\gamma_{C3} = 0.6055$. Red curves (online) are isotherms according to the classical van der Waals model. Critical data: $\pi_{C1} = 8.3242 \times 10^{-4}$, $\tau_{C1} = 0.0327$, $\gamma_{C1} = 0.0678$; $\pi_{C2} = 0.1096$, $\tau_{C2} = 0.2297$, $\gamma_{C2} = 0.2060$; $\pi_{C3} = 0.1799$, $\tau_{C3} = 0.1746$, $\gamma_{C3} = 0.6214$. Model parameter set: $A = 2.272$, $U_R/U_A = 2$, $B_s = 10.2898$, $B_s/B_h = 4.913$.

Table 1. Vapor–liquid equilibrium data for TIP5P water obtained from Gibbs ensemble Monte Carlo simulations [51] and calculated with the IAPWS-95 formulation [48].

T (K)	ρ_{liquid} (kg m^{-3})	P_{MC} (MPa)	$P_{IAPWS-95}$ (MPa)	RD (%)
298.15	984	0.0116	0.003 17	266
325	964	0.0366	0.013 53	270
350	941	0.112	0.041 68	272
375	908	0.276	0.108 30	155
400	864	0.593	0.245 77	141
425	822	1.17	0.500 25	134
450	771	2.18	0.932 20	134
475	703	3.53	1.616 0	119
490	669	4.92	2.183 1	125

about the second critical point parameters in water should be guided by experimental data but not the computer simulations of 'water like' models.

The very wide temperature range measurements of the density of water by Mallamace *et al* [39] found out the well defined minimum in the metastable supercooled phase at 203 ± 5 K (inset in figure 9), in agreement with computer simulations and the van der Waals like models depicted in figure 5 (the expanded scale presented in figure 9). The appearance of minimum and maximum densities at the isobar leads to the intersection of the three isotherms at given density in the P–ρ phase diagram (figure 9). This fact denotes the possible appearance of the reverse LDL–HDL coexistence curve relative to the position of the gas–LDL coexistence curve (figure 10). The appearance of a density anomaly is also confirmed in the computer simulation of a continuous soft core attractive potential by Franzese [53].

To estimate the position of possible critical points in water we have analyzed the behavior of the Widom lines in the wide temperature range at different pressures on the basis of the IAPWS-95 EoS. The well-known property of water to have its isobaric heat capacity maximum in the vicinity of 37 °C forms an uncomplicated extrapolation behavior of C_P^{max} at high pressures (figure 8). The other region where the appearance of the Widom line exists is in the metastable part of the phase diagram at low temperatures. The extrapolation of available experimental data and qualitative rescaled results of computer simulations demonstrated that the function C_P^{max} is weakly dependent on temperature and its definitional domain has a sense in the pressure interval from 0 until ∼25 MPa. The

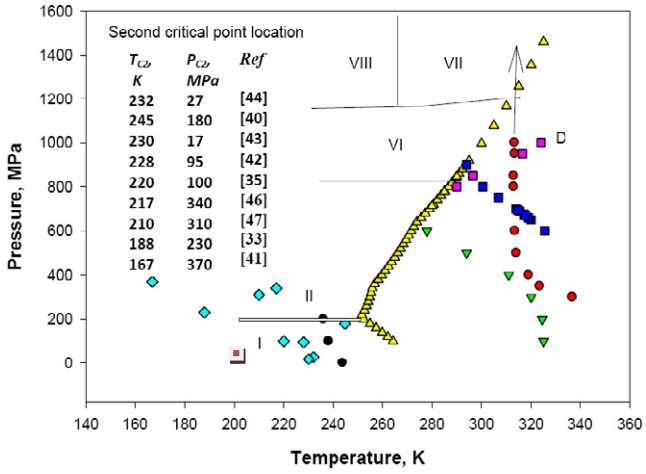

Figure 8. The loci of extreme behavior of isothermal compressibility, isobaric heat capacity, and thermodynamic derivatives. The symbols from the right side of the melting line (yellow triangles— △) correspond to the values $C_P^{\max}$ (●), $k_T^{\min}$ (▲), $(\frac{\partial P}{\partial \rho})_T^{\max}$ (■), and thermal diffusivity (■) calculated with the IAPWS-95 formulation [48]. The symbols from the left side of the melting line correspond to values $C_P^{\max}$ (●) from MD calculations for the TIP5P interaction potential [49], the most credible theoretical forecasts of the second critical point (◆). The hypothesized second critical point from the present study (■)

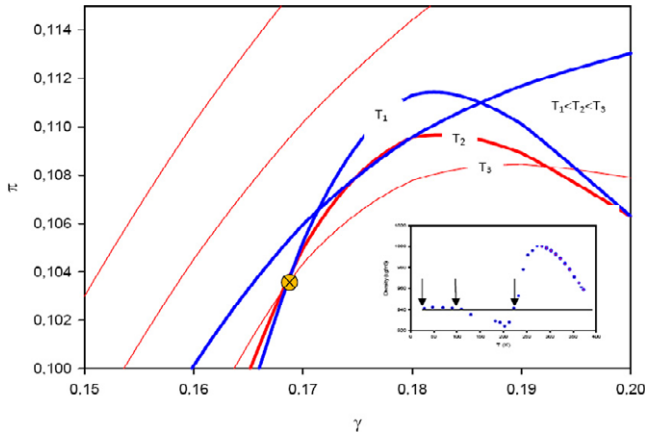

Figure 9. Appearance of the density anomalies of water at low temperatures and the intersection of the isotherms in the metastable region. In the inset, the experimental data [39] and appearance of three values of temperature with the same densities at the isobar are shown.

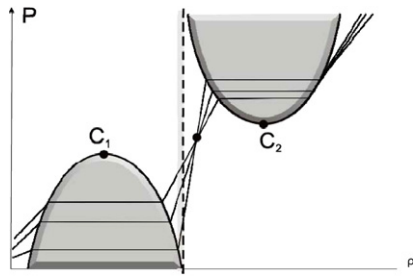

Figure 10. The P–ρ phase diagram. C_1 is the critical point of the gas–LDL phase transition; C_2 is the second critical point of the LDL–HDL phase transition. Dashed line illustrates a melting curve location.

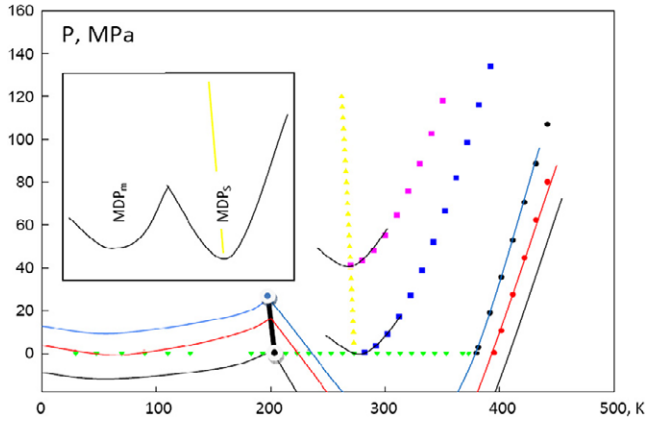

Figure 11. Experimental and hypothetical isochores for water in low temperature region. The densities are 1020 kg m^{-3} (■), 1000 kg m^{-3} (■), 953 kg m^{-3} (●), 941 kg m^{-3} (●), 924 kg m^{-3} (the brown line) was taken from [48]. The lines with the same colors correspond to the continuation and interpolation of the densities mentioned. The yellow color (online) is the melting curve. A schematic global behavior of the isochore is given in the inset. The MDP_S and MDP_m denote the maximum density points for stable and metastable phases, respectively. The hypothesized reverse λ-line is sketched out by the heavy line.

weak divergence in the vicinity of the liquid–liquid critical point suggests a slight difference among $C_P^{\max}$, $k_T^{\max}$ curves, and the critical isochore. The intersection of these lines defines a critical point with high accuracy. The $C_P^{\min}$, $k_T^{\min}$ positions in the temperature range 250–320 K at pressures up to 50 MPa practically coincide and the same picture is repeated for the $C_P^{\max}$, $k_T^{\max}$ in the vicinity of the density minimum at 203 K. The largest values of the $C_P^{\max}$, $k_T^{\max}$ are observed when $P \to 0$. In contrast to the gas–liquid phase transition the values of thermodynamic response functions diverge weakly near the liquid–liquid critical point. This suggests that the isochore behavior reconstructed from the data of Mallamace *et al* [39] and the IAPWS-95 EoS bears a strong resemblance to the isochore behavior at the phase transition HeI–HeII in the reverse scale of pressures. This assumption forecasts the availability not only of the second critical point but also of the λ-line for the liquid–liquid phase transition. The location of this line is restricted by the temperature boundaries 203 ± 5 K within pressures range from negative pressures up to 25 MPa. The uncertainty of the λ-line position is practically indistinguishable in comparison with the second critical point predictions of different authors (figure 8). To confirm this viewpoint experiments on the characterization of the λ-line slope are required.

A similar analysis of the Widom line data can be applied to an estimation of the third critical point. From figure 8 it is possible to establish a tendency in the behavior of the $C_P^{\max}$ curve at high pressures. The continuation of the $C_P^{\max}$ line lies in the temperature range 313–320 K for $P >$ 400 MPa (figure 8). The search for the desired intersection for the Widom lines $C_P^{\max}$ and $k_T^{\max}$ is impossible for the

temperature range of interest because the maximum isothermal compressibility appears only at $T > T_{C1}$. To find the Widom line intersection we have used instead of the k_T^{max} line the critical isochore. For the determination of the critical isochore we carried out a search of such isochores where 'the initial docking contact' of the isochores in metastable states along a melting line (figure 11) with the C_P^{max} line looks like a peak. The minimum value of the density, where the most distinct point of beak-generating contact is observed, was characterized by the next parameter set that one can identify as the third critical point ($T_{C3} \approx 320$ K, $\rho_{C3} \approx 1315$ kg m^{-3}, $P_{C3} \approx 2000$ MPa). This result corresponds to the parameters of state observed for the HDL and VHDL phases [54] and confirms the qualitative forecast of the van der Waals like EoS for the locations of the critical points in the P–T phase diagram.

Acknowledgments

We thank G Franzese, F Mallamace, A Drozd-Rzoska, S Rzoska, and J Tamarit for helpful discussions and assistance. The research is partly supported by the NATO Collaborative Linkage Grant CBP NUKR. CLG 982312 and a grant MK 06/04F from the Ministry of Education and Science of Ukraine.

References

[1] Van Thiel M and Ree F 1993 *Phys. Rev.* B **48** 3591
[2] Togaya M 1997 *Phys. Rev. Lett.* **79** 2474
[3] Katayama Y, Mizutani T, Utsumi W, Shimomura O, Yamakata M and Funakoshi K 2004 *Nature* **403** 170
[4] Katayama Y, Inamura Y, Yamakata M, Mizutani T, Utsumi W and Shimomura O 2004 *Science* **306** 848
[5] Monaco G, Falconi S, Crichton W and Mezouar M 2003 *Phys. Rev. Lett.* **90** 255701
[6] Tanaka H, Kurita R and Mataki H 2004 *Phys. Rev. Lett.* **92** 025701
[7] Kurita R and Tanaka H 2004 *Science* **306** 845
[8] Angell C, Borick S and Grabow M 1996 *J. Non-Cryst. Solids* **207** 463
[9] Mukherjee G and Boehler R 2007 *Phys. Rev. Lett.* **99** 225701
[10] Mishima O and Stanley H E 1998 *Nature* **396** 329
[11] Bellissent-Funel M-C 1998 *Nuovo Cimento* D **20** 2107
[12] Soper A and Ricci M 2000 *Phys. Rev. Lett* **84** 2881
[13] Suzuki Y and Mishima O 2002 *Nature* **419** 599
[14] Loerting T, Salzmann C, Kohl I, Mayer E and Hallbrucker A 2001 *Phys. Chem. Chem. Phys.* **3** 5355
[15] Fomin Yu, Ryzhov V and Tareeva E 2006 *Phys. Rev.* E **74** 041201
[16] Cervantes L, Benavides A and del Rio F 2007 *J. Chem. Phys.* **126** 084507
[17] Poole P H, Sciortino F, Grande T, Stanley H E and Angell C A 1994 *Phys. Rev. Lett.* **73** 1632
[18] Truskett T M, Debenedetti P G, Sastry S and Torquato S 1999 *J. Chem. Phys.* **111** 2647
[19] Jeffrey C A and Austin P H 1999 *J. Chem. Phys.* **110** 484
[20] Skibinsky A, Buldyrev S, Franzese G, Malescio G and Stanley H E 2004 *Phys. Rev.* E **69** 061206
Franzese G, Malescio G, Skibinsky A, Buldyrev S and Stanley H E 2001 *Nature* **409** 692
Franzese G, Malescio G, Skibinsky A, Buldyrev S and Stanley H E 2002 *Phys. Rev.* E **66** 051206
Malescio G, Franzese G, Skibinsky A, Buldyrev S and Stanley H E 2005 *Phys. Rev.* E **71** 061504
[21] Borick S, Debenedetti P G and Sastry S 1995 *J. Phys. Chem.* **99** 3781
[22] Roberts C J and Debenedetti P G 1996 *J. Chem. Phys.* **105** 658
[23] Franzese G and Stanley H E 2002 *J. Phys.: Condens. Matter* **14** 2201
Franzese G, Malescio G, Skibinsky A, Buldyrev S and Stanley H E 2002 *Phys. Rev.* E **66** 051206
Malescio G, Franzese G, Skibinsky A, Buldyrev S and Stanley H E 2005 *Phys. Rev.* E **71** 061504
[24] Ponyatovsky E G, Sinitsyn V V and Pozdnyakova T A 1994 *JETP Lett.* **60** 360
[25] Moynihan C T 1997 *Mater. Res. Soc. Symp. Proc.* **455** 411
[26] Ponyatovsky E G and Sinitsyn V V 1999 *Physica* B **265** 121
[27] Sasai M 1990 *J. Chem. Phys.* **93** 7329
[28] Tanaka H 1998 *Phys. Rev. Lett.* **80** 5750
[29] Tanaka H 1999 *J. Phys.: Condens. Matter* **11** L159
[30] Tanaka H 2000 *Europhys. Lett.* **50** 340
[31] Tanaka H 2000 *J. Chem. Phys.* **112** 799
[32] Tanaka H 2000 *Phys. Rev.* E **62** 6968
[33] Kiselev S and Ely J 2002 *J. Chem. Phys.* **116** 5657
[34] Hemmer P and Stell G 1970 *Phys. Rev. Lett.* **24** 1284
[35] Mishima O and Stanley H E 1998 *Nature* **392** 164
[36] Debenedetti P 2003 *J. Phys.: Condens. Matter* **15** R1669
[37] Loerting T and Giovambattista N 2006 *J. Phys.: Condens. Matter* **18** R919
[38] Liu H 2006 *Preprint* cond-mat/0605392
[39] Mallamace F, Branca C, Broccio M, Corsaro C, Mou C-Y and Chen S-H 2007 *Proc. Natl Acad. Sci. USA* **104** 18387
[40] Giovambattista N, Stanley H E and Sciortino F 2005 *Phys. Rev. Lett.* **94** 107803
[41] Truskett M, Debenedetti P, Sastry S and Torquato S 1999 *J. Chem. Phys.* **111** 2647
[42] Jeffery C and Austin P 1999 *J. Chem. Phys.* **110** 484
[43] Ponyatovsly E, Synitsyn V and Pozdnyakova T 1998 *J. Chem. Phys.* **109** 2413
[44] Fuentevilla D and Anisimov M 2006 *Phys. Rev. Lett.* **97** 195702
[45] Saika-Voivod I, Sciortino F and Poole P H 2004 *Phil. Mag.* **84** 1437
[46] Yamada M, Mossa S, Stanley H E and Sciortino F 2002 *Phys. Rev. Lett.* **88** 195701
[47] Paschek D 2005 *Phys. Rev. Lett.* **94** 217802
[48] Wagner W and Pruß A 2002 *J. Phys. Chem. Ref. Data* **31** 387
[49] Gray C, Goldman S, Tomberli B and Li W 1997 *Chem. Phys. Lett.* **271** 185
Franzese G and Stanley H E 2007 *J. Phys.: Condens. Matter* **19** 205126
Kumar P, Franzese G and Stanley H E 2008 *Phys. Rev. Lett.* **100** 084102
[50] Mahoney M and Jorgensen W 2000 *J. Chem. Phys.* **112** 8910
[51] Lisal M, Kolafa J and Nezbeda I 2002 *J. Chem. Phys.* **117** 8892
[52] Xu L, Kumar P, Buldyrev S, Chen S-H, Poole P, Sciortino F and Stanley H E 2005 *Proc. Natl Acad. Sci. USA* **102** 16558
[53] Franzese G 2007 *J. Mol. Liq.* **136** 267
[54] Giovambattista N, Stanley H E and Sciortino F 2005 *Phys. Rev. Lett.* **94** 107803